

LSST All-Sky IR Camera Cloud Monitoring Test Results

Jacques Sebag^a, John Andrew^a, Dimitri Klebe^b, Ronald D. Blatherwick^c

^a National Optical Astronomical Observatory, 950 N Cherry, Tucson AZ 85719

^b Denver Museum of Nature and Science, 2001 Colorado Blvd, Denver CO 80205

^c University of Denver, 2112 E. Wesley Ave., Denver, CO 80208

ABSTRACT

The LSST project has updated the all-sky IR camera that was installed on Cerro Pachón in Chile to continue its investigations in cloud monitoring and quantifying photometric conditions. The objective is to provide the survey scheduler with real-time measured conditions of the sky/clouds, including high cirrus to better optimize the observing strategy. This paper describes the changes done to improve the detection performance of the first generation system and presents comparison results of visible and IR images. Contemporaneous visible measurements of extinction taken with the 1.2m Calypso Telescope on Kitt Peak are also provided.

Keyword:

All-Sky Camera, IR Camera, Cloud Monitoring

1. INTRODUCTION

The Large Synoptic Survey Telescope (LSST) has been evaluating the use of visible and infrared all-sky cameras as sources of cloud cover data to inform the scheduling process. The system presented here is an upgraded unit of the instrument described in [1], known as ASIVA for All-Sky Infrared Visible Analyzer, which includes a specially designed 180deg cone angle refractive lens that makes the overall system relatively compact. The original unit and the upgrade were purchased from the Solmirus Corporation.

A new 8-14 micron IR detector was installed to replace the 320x240 pixel array Barium-Strontium-Titanate (BST) infrared detector. This previous detector proved to be difficult to calibrate because the array is modulated through the use of a chopper wheel in order to measure the temporal change of temperature on the detector. The chopper wheel operates in such a way that the individual pixel radiation was referenced to that of the pixel's immediate surroundings. This characteristic made absolute radiometric calibration unattainable. Other internal changes were also added to improve the calibration and the archiving of the data.

The upgraded unit is being tested on Kitt Peak in Arizona. It is located near the Calypso Telescope (figure 1) in order to compare visible images taken with Calypso and IR images. This report provides a short overview of the upgraded instrument, the revised calibration process, and the results obtained so far on the data acquired during these tests.

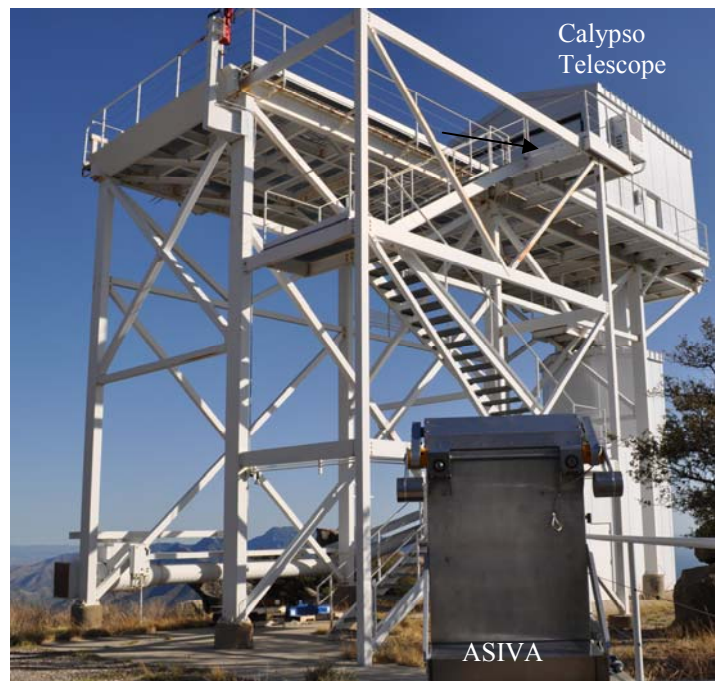


Figure 1: ASIVA next to the Calypso Telescope on Kitt Peak

2. DESCRIPTION OF THE UPGRADED INSTRUMENT

This section is focused on the main system upgrades (see [1] for general description of the instrument). Replacing the IR camera was the main driver for this upgrade. The new uncooled infrared camera is a Photon 640 model developed by FLIR. It contains a 640x512 pixel array microbolometer infrared detector with 25-micron square pixels and the camera has a 30Hz frame rate. Based on the camera specifications, the Noise Equivalent Temperature Difference (NETD) performance is expected around 0.05degK or less per frame. The images are digitized inside the camera into a 14bit digital output. This new camera brings a factor 4 better spatial resolution thanks to its smaller pixel size without reducing the field of view due to the array's larger form factor. Another significant change is the detection performance which is improved by a factor 4.

Detector	640 x 512 pixels
Pixel Size	25-micron square pixel
Total detector area	16mm x 12.8mm
Objective lens focal ratio	1.4
Objective focal length	5.9mm
NETD	0.050 deg K or less

Table 1: ASIVA New Camera Main Characteristics

The set of six filters (F1 to F6) was modified to include two new filters (figure 2), one of them being custom designed to cover the 10.2 to 12.2 micron atmospheric window. This filter completes the previous filter set to help in identifying the different effects of atmospheric emission. In particular, the spectral radiance ratio of these two filters may provide a gauge to the amount of precipitable water vapor.

The visible camera and lens was also changed in the new system with a progressive scan interline CCD detector array of 1392x1040 pixels with a pixel size of 4.65x4.65 μm^2 and equipped with an LP550 longpass filter with a cut-off around 550nm. The transparent dome that was permanently mounted above the visible camera was removed to improve the image quality and was replaced with a hatch mechanism that covers the lens for protection when not used. This mechanism was designed to provide a weather tight protection for both channels (IR and visible). It includes a drive motor with a worm-gear reduction and a custom dual chain system for additional speed reduction. Two redesigned blackbodies are built inside the hatch (one for each channel) for the calibration of the images.

The previous user interface was retired and replaced with command scripts for the acquisition and analysis of the data.

An observing script governs the data acquisition sequence for the filters and the exposure time, and all the images are saved as FITS files. Each sequence begins with the hatch closed. An IR blackbody reference image as well as a visible dark reference image are acquired in that position. The hatch is then opened and sky images are acquired until the next sequence starts. Every IR image has 1.6sec exposure duration and eight images are stored together in a 3D FITS data cube file for a total exposure duration of 12.8seconds. A process script analyzes the acquired images and creates the data products that are stored into a single web database.

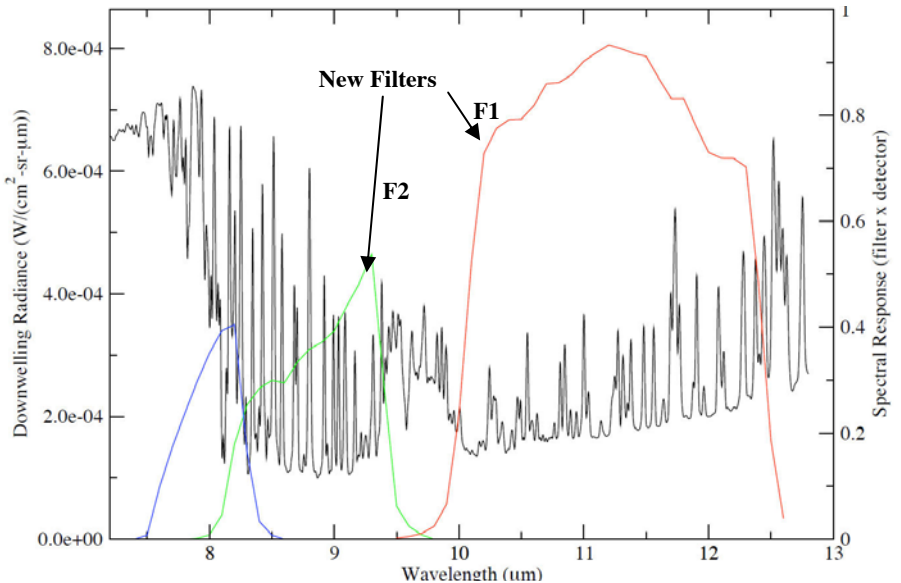


Figure 2: New filters spectral response on top of clear-sky downwelling radiance computed with MODTRAN

2. CALIBRATION

The built-in blackbody reference located inside the hatch cover is used to determine the instrumental response of the system and also to measure the fixed pattern components in the image. In this model, three temperature sensors (RTD) are bonded on the back of the blackbody near the emissive surface (T1 near the center, T2 in the middle and T3 at the edge). A heater was also added on the back surface of the blackbody to control its temperature during calibration. In normal operation, the hatch is usually opened and the blackbody temperature simply follows the outside air temperature. The hatch is closed in between each set of images and a reference image is taken for each filter. For the calibration, the blackbody is heated with the hatch in the open position until reaching a temperature of 80degC. Then, the heater is turned off and images are taken for all filters by closing and opening the hatch for different blackbody temperatures during the cooling down period. This method was chosen to avoid heating of the IR lens during the calibration procedure.

The pixel instrument response coefficients G_λ are determined to convert the raw data images into brightness temperature or flux calibrated images. They are calculated for each specific filter by applying the following equation:

$$G_\lambda = \frac{I_\lambda(T)}{\varepsilon_\lambda \cdot BB_\lambda(T)} \text{ in [counts per W/m}^2\text{/m/sr]} \quad (1)$$

where

I_λ is the pixel count value for each blackbody temperature and for each filter image

ε_λ is the emissivity of the blackbody

$BB_\lambda(T)$ is the radiance for the blackbody at each temperature and integrated over the bandwidth of each filter
The radiance from a blackbody is given by the Planck function

$$B_\lambda = \frac{2hc^2}{\lambda^5} \frac{1}{(e^{\frac{hc}{k\lambda T}} - 1)} \quad \text{in } Wm^{-2}sr^{-1} m^{-1} \quad (2)$$

and $BB_\lambda(T)$ is computed as

$$BB_\lambda(T) = \int B_\lambda \cdot t_\lambda d\lambda / \int t_\lambda d\lambda \quad \text{in } Wm^{-2}sr^{-1} m^{-1} \quad (3)$$

where c is the speed of light, h is the Planck constant, λ is the wavelength, k is the Boltzmann constant and T is the temperature. The radiance is integrated over each filter bandwidth using t_λ the filter bandpass as a function of wavelength. The instrument response versus integrated radiance for one particular pixel is shown on figure 3 for filter 1.

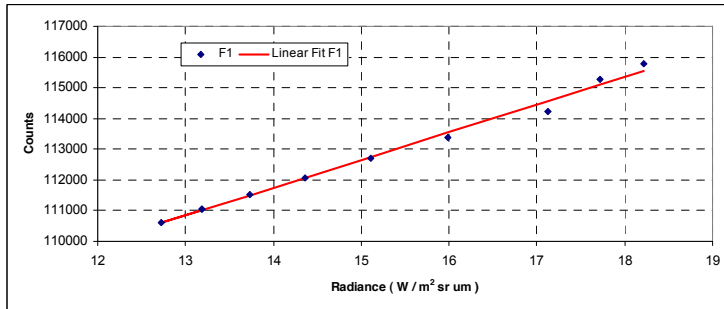


Figure 3: Instrument Response versus Integrated Radiance for filter 1

Images of an external blackbody were also acquired for each different filter to verify the calibration process. This blackbody provided a large enough circular aperture to create a 10-pixel diameter spot on the image. The controlled blackbody temperature was stepped between 50degC and 100degC. All these images were flux calibrated and the radiance measured in each image was compared to the computed radiance based on the blackbody temperature.

The results for filter 1 are given in table 2. Reasonable differences (~1-2%) were obtained between 50 and 80degC but the

radiance difference at 100degC was larger than expected, suggesting that there is a possible slight error in the estimation of the pixel instrument response or a departure from linearity at this temperature. Another calibration campaign is planned in the future with a different range of temperatures to verify the current instrument response.

Temperature T (degC)	50	65	80	100
BB(T) Computed Radiance filter 1 (W/m ² sr m)	12.82	15.37	18.16	22.23
BB(T) Measured Radiance filter 1 (W/m ² sr m)	12.59	15.27	18.37	23.10
[Measured-Computed] Radiance Difference (W/m ² sr m)	-0.23	0.10	0.21	0.87
Ratio of Radiance Difference over Measured Radiance	1.9%	0.6%	1.1%	3.7%

Table 2: External blackbody flux calibration

3. CLOUD DETECTION AND SKY QUALITY

Multiple data products are generated from the raw images to determine the presence of clouds and the photometric sky quality. To monitor the sky cloud level, a sky quality image is created using a combination of the data products where a value is computed for each pixel on a scale of 0 to 1, with 0 being photometric and 1 being completely cloudy or highly variable. From these images, a zenith sky quality value and a total sky quality value are also computed. These quantities represent the average sky quality over the pixels located in the central 30degree cone and in the 150degree cone. The variations of both parameters are given in figure 4 for three different nights during clear, mixed and cloudy sky conditions with an increasing sky quality scale from top to bottom plot to display small changes.

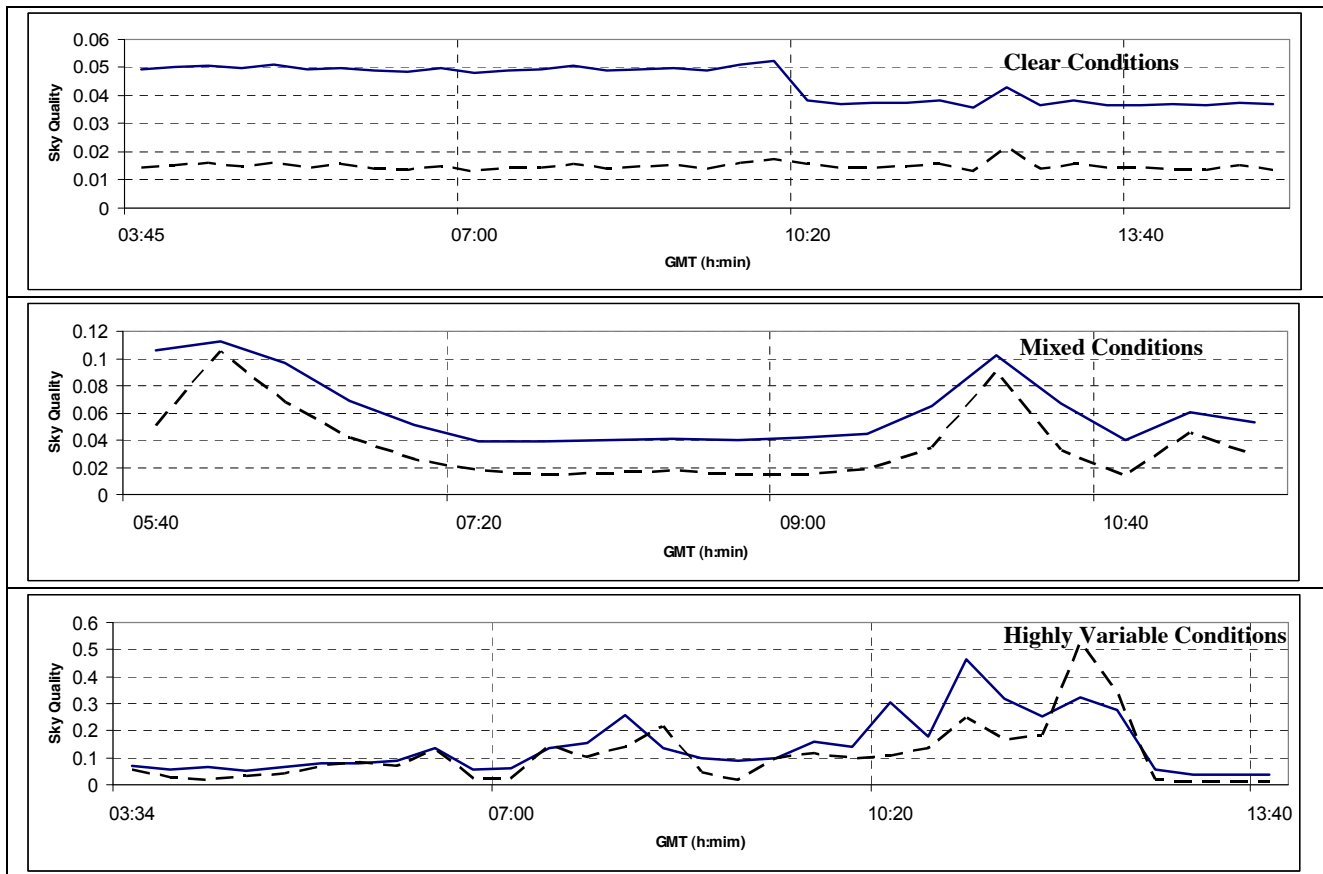


Figure 4: Examples of three nights showing total quality (continuous line) and zenith quality (dash line) values for clear conditions (top), mixed conditions (middle) and highly variable cloudy conditions (bottom). The scale for the sky quality on the y-axis increases gradually from top to bottom plot to show small details.

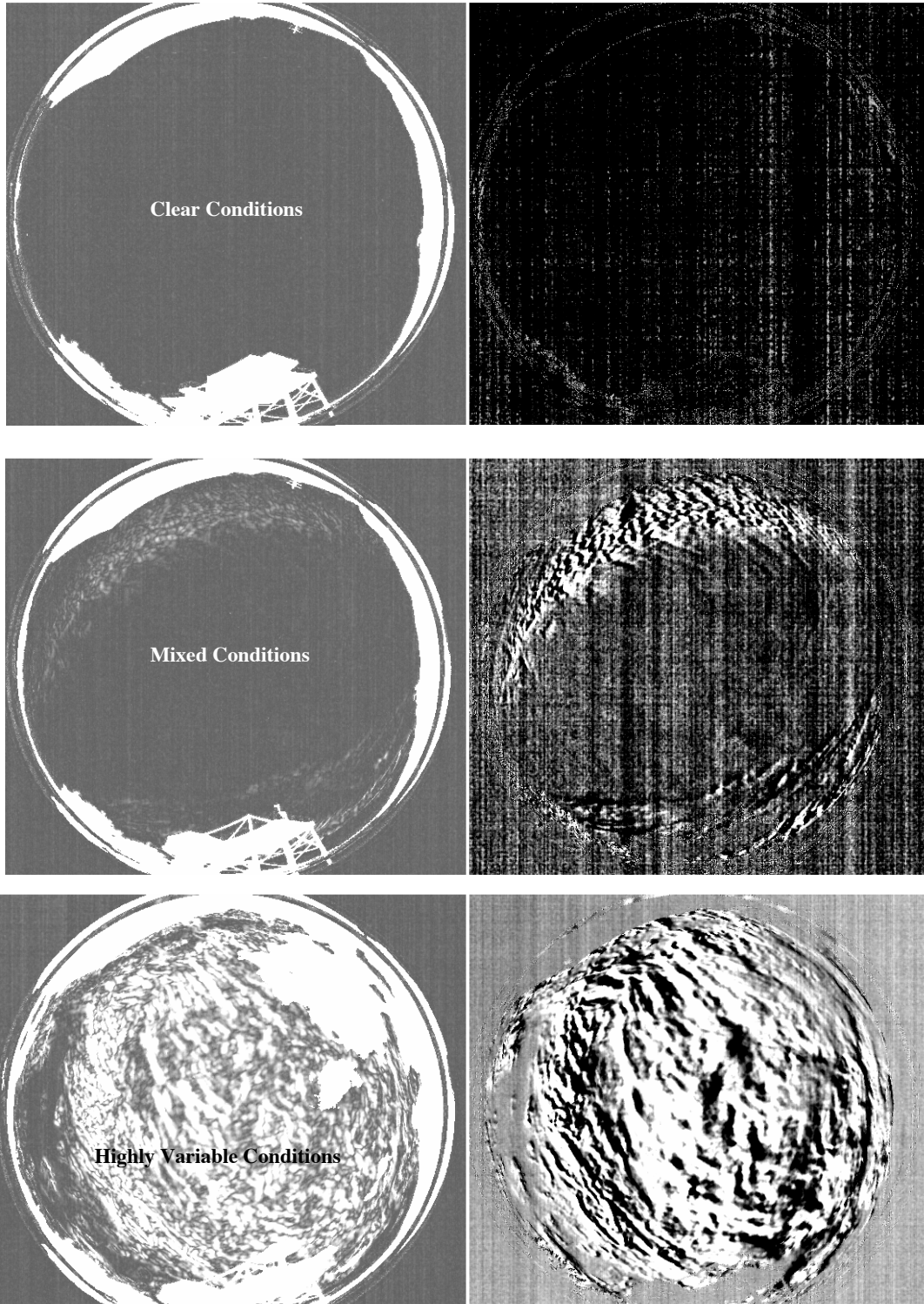


Figure 5: Images taken during the same nights as figure 3 showing sky quality images (left side) and temporal difference images (right side) at the following specific time of 7:00 GMT (top), 10:40 GMT (middle) and 8:00 GMT (bottom).

Both parameters are very sensitive to the presence of clouds. In clear conditions, they are very close to zero, with the zenith sky quality value being very stable around 0.015. The total sky quality value is usually around 0.04 for similar conditions. However, variations near the horizon may interfere at the edge of the 150deg cone angle making this parameter not as stable as the zenith sky quality. Clouds coming from one direction would first increase the value of the total sky quality and then would impact the zenith sky quality upon entering the area defined by the smaller cone angle. Images taken during each of these nights are shown in figure 5, with the sky quality image on the left side. The Calypso Telescope is the structure at the bottom of the image, with the clear sky background dark and the clouds in white. The images on the right side were obtained by computing the difference between image 1 and 8 in the 3D FITS data cube. These images are separated by an 11 second time interval. The pattern visible on the difference image is due to the displacement of the clouds during that time interval. This displacement is helpful for cloud detection as the contrast is amplified near the edge of the clouds by the image differencing process. Moreover, these difference images could be analyzed to determine the speed and direction of the clouds.

The sky quality parameter is also an indicator of the thickness/altitude of the clouds. A high value indicates clouds that are thick or at low altitude. These are the type of clouds that are usually detectable by an observer that would declare cloudy weather conditions. Table 3 shows the expected integrated radiance range per filter that the instrument should measure in the flux calibrated images for thick clouds that would behave like blackbodies between 0degC and 10degC. The comparison between measured radiance and sky quality is in progress to take into account the radiance for the different filters and to determine the amount of precipitable water vapor (PWV) (see discussion below).

Filter	F1	F2	F3	F4	F5	F6
208K blackbody Integrated Radiance ($Wm^{-2} sr^{-1} m^{-1}$)	1.39	0.89	1.23	1.14	0.65	1.49
273K blackbody Integrated Radiance ($Wm^{-2} sr^{-1} m^{-1}$)	6.11	5.68	6.03	6.10	5.02	6.00
283K blackbody Integrated Radiance ($Wm^{-2} sr^{-1} m^{-1}$)	7.23	7.01	7.23	7.37	6.33	7.03

Table 3: Integrated radiance per filter in ASIVA for a blackbody at -65degC (208degK) representative for clear sky conditions and thick clouds at 0degC (273degK) and 10degC (283degK)

For the purpose of our tests, the most interesting set of images is when the sky quality is in the mixed regime with values around 0.1. Our goal is to be able to detect thin cirrus with a low IR optical depth (down to 0.01) that are found at higher altitudes and are usually not detectable by an observer. Figure 6 gives an example of such conditions by showing two sets of sky quality and visible images taken during the same night within a 40min time interval. The visible image was acquired at the same time as the sky quality image using the visible camera in the ASIVA system. In the first set of images, the presence of clouds is only visible toward the horizon in the sky quality image and the sky is clear of clouds at zenith. The zenith sky quality is found equal to 0.01. In the visible image, the sky appears completely clear showing the Milky Way and multiple stars over the whole visible sky. In the second set of images, clouds are now clearly visible at zenith and the zenith sky quality parameter is found equal to 0.09 which indicates that these clouds may not be easily detectable in the visible images. For that example, the clouds are not detectable by comparing visually both set of visible images. In most cases, the radiance of the thin cloud with a 0.01 IR optical depth is high enough that it should be detected with the new camera with a signal to noise ratio (SNR) around 10. The radiance per filter of such a cloud at a 0degC temperature is shown on table 4.

Filter	F1	F2	F3	F4	F5	F6
Thin cloud radiance with a 0.01 optical depth ($mWm^{-2} sr^{-1} m^{-1}$)	61	57	60	61	50	60
Thin cloud detection SNR	9	2	11	3	1	4

Table 4: Radiance of a thin cloud with a 0.01 optical depth for the different filters in ASIVA and detection signal to noise ratio (SNR)

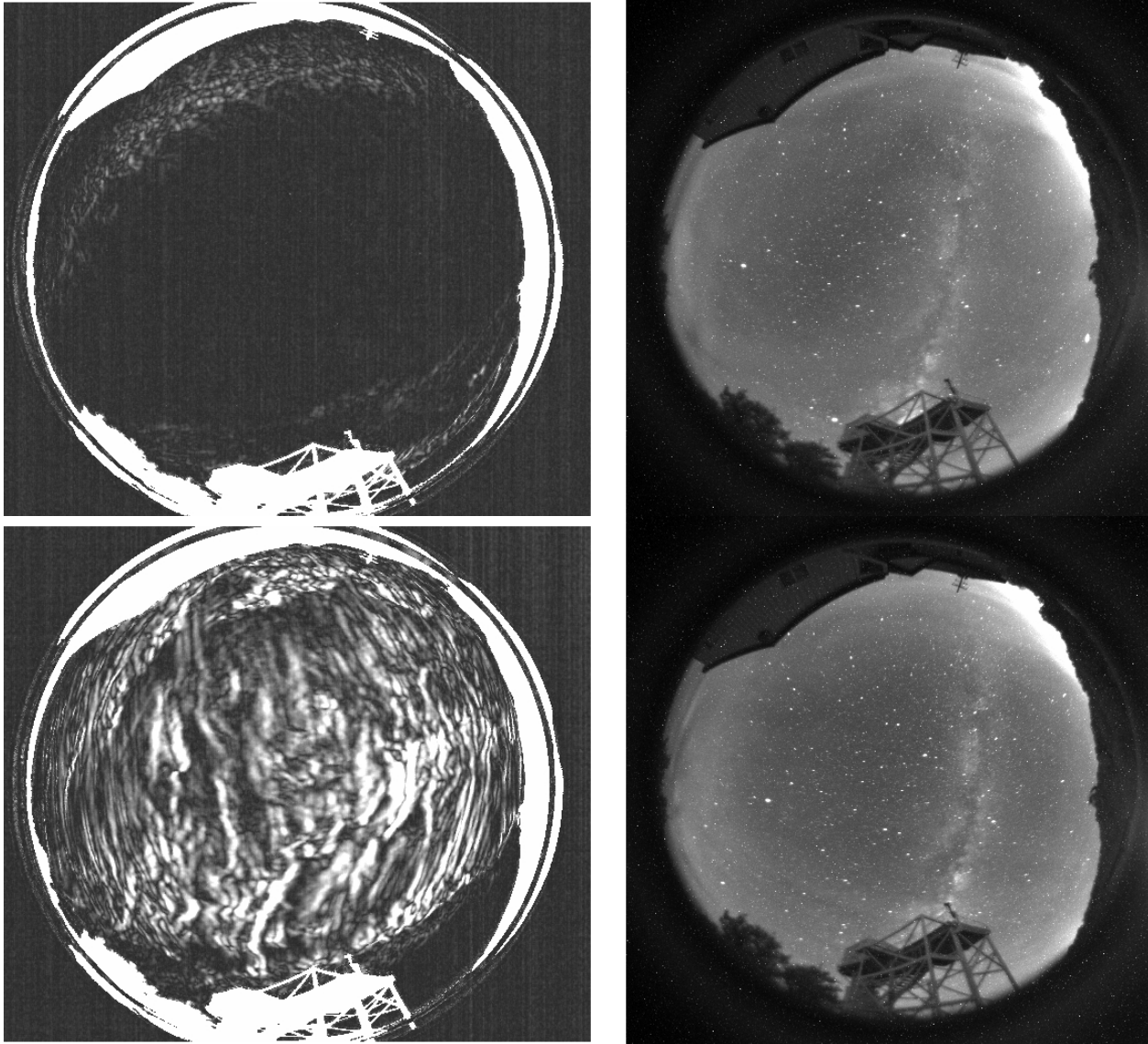


Figure 6: Sky quality images (left side) and visible images (right side) taken at the same time.

4. WATER VAPOR DETERMINATION

The filters included in the ASIVA instrument provide a unique capability for measuring the all-sky emission in different wavebands. Three of these wavebands (Filter 1 (10 to 12 μm), Filter 2 (8 to 9.5 μm) and Filter 5 (7.5 to 8.4 μm)) are particularly sensitive to emission from atmospheric water vapor. To evaluate this sensitivity, MODTRAN radiative transfer code was used to determine the downwelling radiance as a function of Precipitable Water Vapor (PWV) in the different wavebands. The results of these simulations are illustrated in Figure 7 where the filtered-averaged downwelling radiance (normalized to a blackbody of $T = 300\text{degK}$) is plotted as a function of PWV.

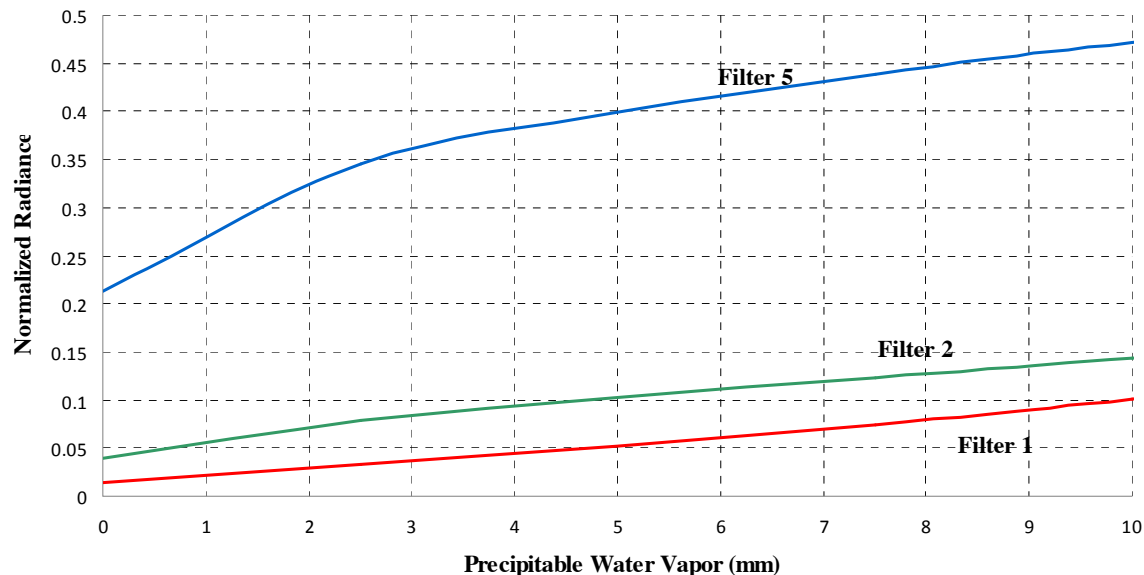


Figure 7: Downwelling Radiance integrated for filters F1, F2 and F5 and normalized by 300degK blackbody radiance as a function of precipitable water vapor

Normalizing the radiance enables a straightforward means of comparing the results of these simulations with ASIVA data which can be normalized to the reference blackbody built into the hatch. As can be seen in Figure 2, Filter 1 offers the best clear sky/cloud radiance wherein clouds will produce a normalized radiance near unity. Filter 5 provides the best sensitivity to PWV but its significantly lower instrumental response may limit its performance in this regard. We are currently investigating results shown in Figure 7 for its potential in determining PWV.

ACKNOWLEDGMENT

The authors have special thanks to the Kitt Peak Staff for their assistance in installing the IR camera near the Calypso Telescope.

LSST is a public-private partnership. Funding for design and development activity comes from the National Science Foundation, private donations, grants to universities, and in-kind support at Department of Energy laboratories and other LSSTC Institutional Members. Work described in this paper is supported by the National Science Foundation under Scientific Program Order No. 9 (AST-0551161) and Scientific Program Order No. 1 (AST-0244680) through Cooperative Agreement AST-0132798.

REFERENCES

1. J. Sebag et al., "LSST IR Camera for Cloud Monitoring and Observation planning", *SPIE Proceedings* Vol. 7012 (2008)